Electromagnetic waves downstream of quasi-perpendicular shocks

Q. M. Lu[1,2] and S. Wang[1]

Received 14 July 2005; revised 10 January 2006; accepted 26 January 2006; published 18 May 2006.

[1] When the incident solar wind H^+ and other minor ions cross a shock, they are decelerated differentially by the electrostatic potential at the shock. Therefore ring beam distributions of the minor ions are formed downstream of a quasi-perpendicular shock in the downstream frame. Moreover, the H^+ distribution downstream of the quasi-perpendicular shock usually has large perpendicular temperature anisotropy. The He^{2+} ring beam distribution and H^+ temperature anisotropy can excite helium cyclotron waves and proton cyclotron waves, respectively. In this paper, we perform one-dimensional hybrid simulations to investigate the competition between the helium cyclotron waves and proton cyclotron waves, and their influences on the evolution of He^{2+} and O^{6+} velocity distributions are also considered. When the wave spectrum is dominated by the helium cyclotron waves, He^{2+} and O^{6+} approximately move on the surface of a sphere, which results in shell-like distributions for $He^{2+}$and O^{6+}. With the increase of the H^+ temperature anisotropy $T_{\perp p}/T_{\|p}$, the amplitude of the proton cyclotron waves also increases. When it is sufficiently large and comparable with that of the helium cyclotron waves, the motions of He^{2+} and O^{6+} are irregular, which results in bi-Maxwellian distributions of $He^{2+}$and O^{6+}. We also investigate the influence of the plasma $\beta_{\|p}$ on the excited ion cyclotron waves and the evolution of the $He^{2+}$and O^{6+} distributions. The simultaneous observations for He^{2+} and O^{6+} in the downstream of shocks with Active Magnetospheric Particle Tracer Explorers (AMPTE)/CCE spacecraft have demonstrated their shell-like distributions. The observed results verify the existence of the helium cyclotron waves downstream of supercritical quasi-perpendicular shocks.

Citation: Lu, Q. M., and S. Wang (2006), Electromagnetic waves downstream of quasi-perpendicular shocks, *J. Geophys. Res.*, *111*, A05204, doi:10.1029/2005JA011319.

1. Introduction

[2] The incident solar wind H^+ distribution is decelerated when it crosses the Earth's bow shock. For a supercritical quasi-perpendicular shock, a fraction of H^+ is reflected at the shock. When these particles gyrate back toward the shock, they gain energy from the motional electric field and are transmitted through the shock into downstream region. Therefore the H^+ distribution downstream of a supercritical quasi-perpendicular shock has large perpendicular temperature anisotropy [e.g., *Leroy et al.*, 1982; *Sckopke et al.*, 1990; *Brinca et al.*, 1990; *McKean et al.*, 1995a; *Lin and Wang*, 2002; *Liu et al.*, 2005], which provides free energy for the growth of electromagnetic waves. Two different instabilities are known to be driven by the H^+ temperature anisotropy downstream of supercritical quasi-perpendicular shocks [e.g., *Winske and Quest*, 1988; *Yoon*, 1992; *Gary*, 1992; *McKean et al.*, 1992; *Anderson and Fuselier*, 1993; *Anderson et al.*, 1994]. The first is the proton cyclotron instability, a transverse mode that generally has maximum growth rate along the ambient magnetic field. The other is the mirror instability, a compressive mode that propagates obliquely to the ambient magnetic field. With a quasi-linear kinetic theory *Yoon* [1992] found that the mirror waves grow at a slightly faster rate, but the subsequent evolution shows that the proton cyclotron waves saturate at a much larger intensity and are more important. Both of the instabilities lead to magnetic fluctuations at frequencies $\omega < \Omega_p$, where Ω_p is the proton gyrofrequency. Besides H^+, there are still many minor ion species in the solar wind that usually have very low concentrations compared with H^+. Among these minor ion species, He^{2+} is the most common solar wind ion after H^+, which constitutes typically about 4% of the total solar wind ion density in number. Considering the effects of He^{2+}, the mirror mode should dominate the proton cyclotron waves for high-beta ($\beta_{\|p} \geq 1$, where $\beta_{\|p}$ is the proton parallel plasma beta), low-anisotropy conditions ($T_{\perp p}/T_{\|p} \leq 2$, where $T_{\perp p}$ and $T_{\|p}$ denote the H^+ temperatures perpendicular and parallel to the ambient magnetic field, respectively) while the proton cyclotron waves should dominate for low-beta, high-anisotropy

[1]CAS Key Laboratory of Basic Plasma Physics, School of Earth and Space Sciences, University of Science and Technology of China, Hefei, China.

[2]Key Laboratory of Space Weather, Center for Space Science and Applied Research, Chinese Academy of Sciences, Beijing, China.

0148-0227/06/2005JA011319$09.00

Table 1. Simulation Parameters for Runs 1–5

Run	$\beta_{\|\|p}$	$T_{\perp p}/T_{\|\|p}$
1	0.5	1.7
2	0.5	3.0
3	0.2	3.0
4	0.2	5.0
5	0.8	1.0

conditions [*Price et al.*, 1986; *Anderson et al.*, 1991; *Fuselier et al.*, 1991; *Gary et al.*, 1993].

[3] At the same time, because of the different charge-to-mass ratios, the electrostatic potential at the shock causes the incident solar wind H^+ and minor ion distributions (such as He^{2+} and O^{6+}) to slow differentially. Since the minor ions have larger kinetic energy than H^+, virtually all of them will be transmitted through the shock potential. On the basis of these considerations, *Fuselier and Schmidt* [1997] propose a simple injection model. In this model, the shock is considered as an infinitely thin electrostatic potential, which slows H^+ much more than the minor ions because of their larger charge-to-mass ratios. Therefore, in the immediate downstream of the shock, there is a relative velocity between minor ions and H^+ if they have same velocity in the solar wind. These minor ions can be thought as "injecting" into downstream in the downstream frame that moves with the average speed of H^+, and it produces ring beam distributions for the minor ions immediately downstream of the shock. This simple model is tested with observations from the ISEE 1 and 2 spacecraft, and it is found to agree reasonably well for quasi-perpendicular shocks. The ring beam distributions of the minor ions downstream of the quasi-perpendicular shock have also been obtained in hybrid simulations [*Lee and Wu*, 2000; *Lee*, 2001]. Similar to the He^{2+} temperature anisotropy [*Gary et al.*, 1994; *Lu et al.*, 2006], the He^{2+} ring beam distribution can excite helium cyclotron waves, which has been investigated by *Lu and Wang* [2005a] with hybrid simulations. Although the proton cyclotron waves and mirror waves driven by H^+ temperature anisotropy have been extensively studied [*Tanaka*, 1985; *Winske and Quest*, 1988; *Lee et al.*, 1988; *Yoon*, 1992; *Gary*, 1992; *McKean et al.*, 1992, 1995a; *Brinca et al.*, 1990; *Liu et al.*, 2005], the helium cyclotron waves excited by the He^{2+} ring beam distribution in the downstream of quasi-perpendicular shocks and its influence on the evolution of He^{2+} and O^{6+} distributions are paid less attention.

[4] In this paper, we perform one-dimensional (1-D) hybrid simulations to investigate the competition between the proton cyclotron waves and helium cyclotron waves downstream of quasi-perpendicular shocks, and different values of the H^+ temperature anisotropy $T_{\perp p}/T_{\|p}$ and plasma beta $\beta_{\|p}$ are used. The mirror waves are negligible because we only consider the situations with low plasma $\beta_{\|p}$. The proton cyclotron waves and helium cyclotron waves are excited by the H^+ perpendicular temperature anisotropy and He^{2+} ring beam distribution, respectively. *Fuselier et al.* [1988] found that both He^{2+} and O^{6+} have shell-like distributions downstream of shock with Active Magnetospheric Particle Tracer Explorers (AMPTE)/CCE spacecraft observations. *Peterson et al.* [1979] observed that He^{2+} distributions is "depleted" relative to H^+ at low energy in the downstream of shocks, and they interpreted this depletion as an unresolved or filled He^{2+} shell. The implications between the evolution of He^{2+} and O^{6+} velocity distributions and the observations are also discussed.

[5] The paper is organized as follows: In section 2, we describe one-dimensional (1-D) hybrid simulation model.

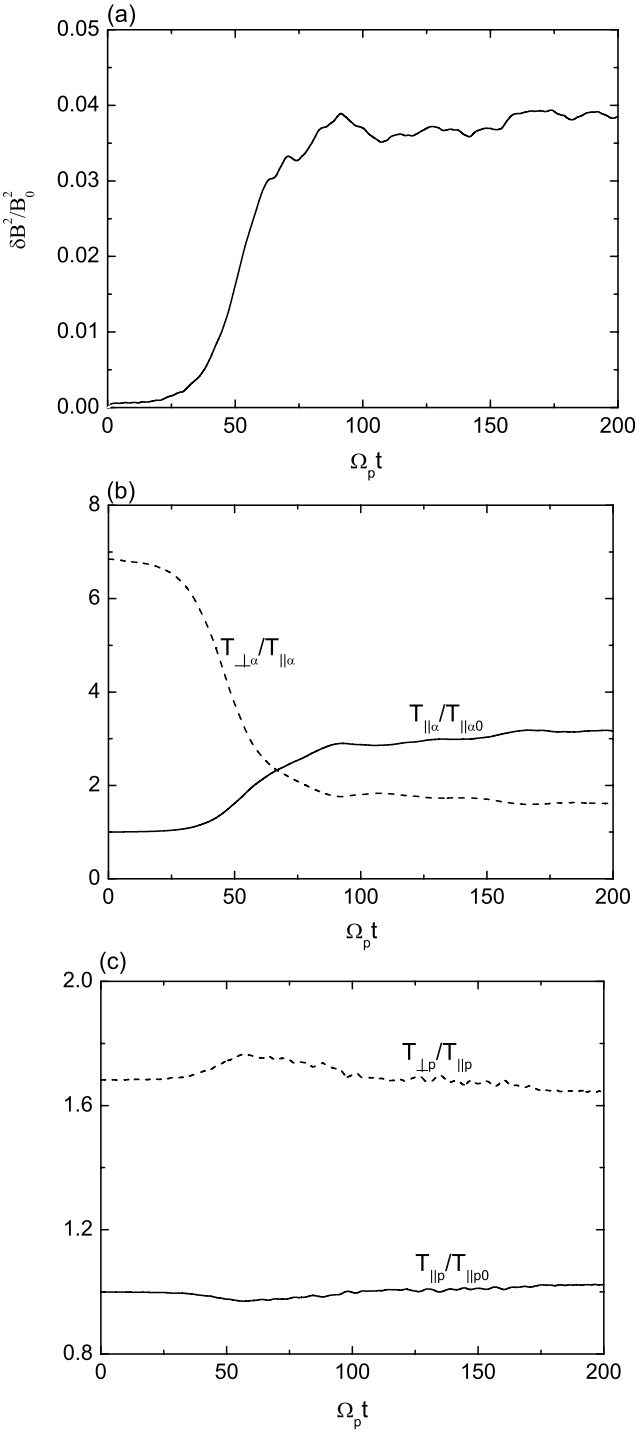

Figure 1. Time evolution of (a) the amplitude of the fluctuating magnetic field $\delta B^2/B_0^2$, (b) the kinetic temperatures for the He^{2+}, and (c) the H^+ temperatures for run 1. $T_{\|\alpha 0}$ and $T_{\|p0}$ are the initial parallel temperatures for He^{2+} and H^+, respectively.

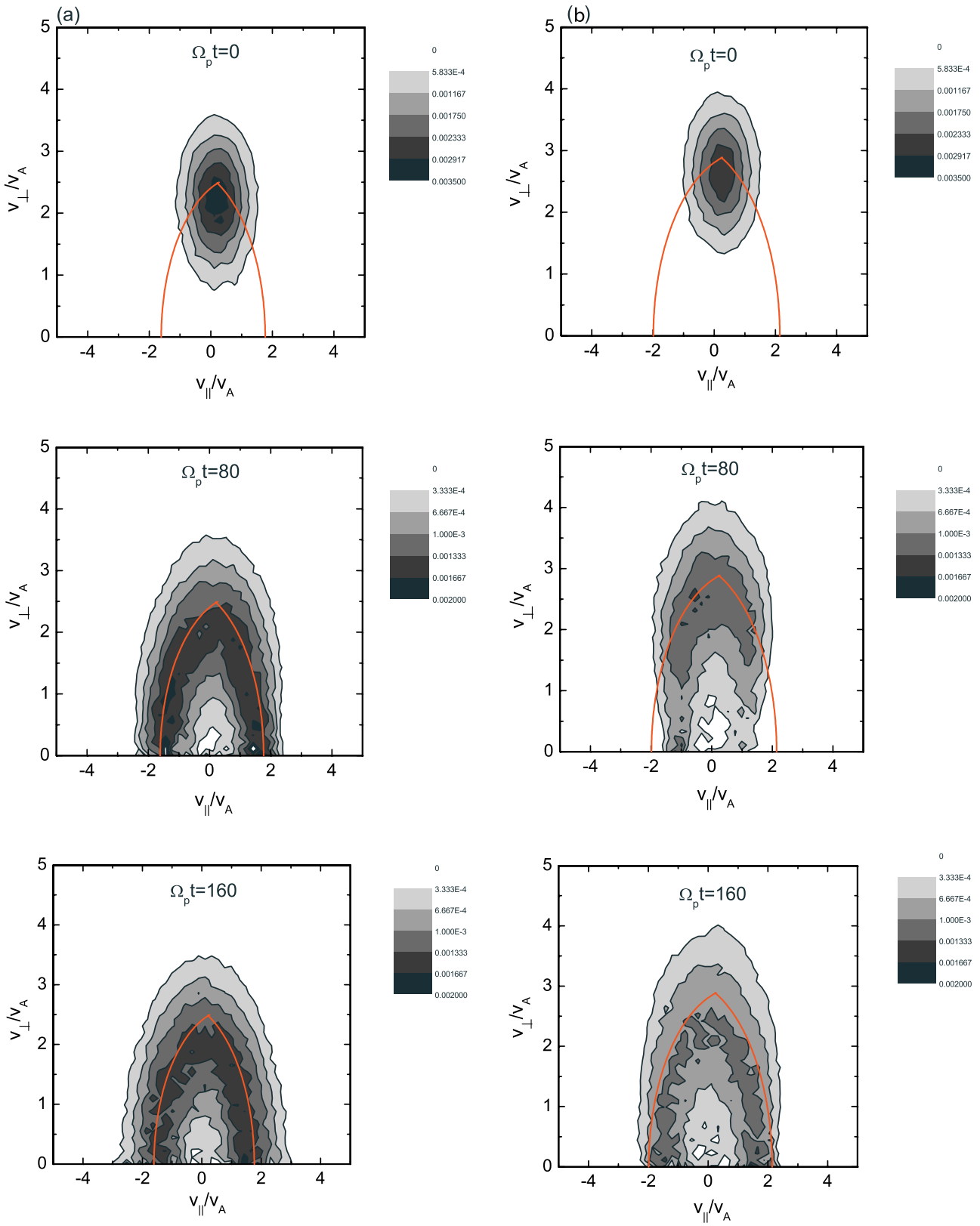

Figure 2. Time evolution of the (a) He^{2+} and (b) O^{6+} velocity distributions $f(v_{||}, v_{\perp})$ at different times for run 1. The red lines denote the He^{2+} and O^{6+} trajectories. The trajectories satisfy equations (4) and (5) at the same time they pass through ($v_{||} = 0.22\ v_A$, $v_{\perp} = 2.49\ v_A$) and ($v_{||} = 0.24\ v_A$, $v_{\perp} = 2.89\ v_A$) for He^{2+} and O^{6+}, respectively.

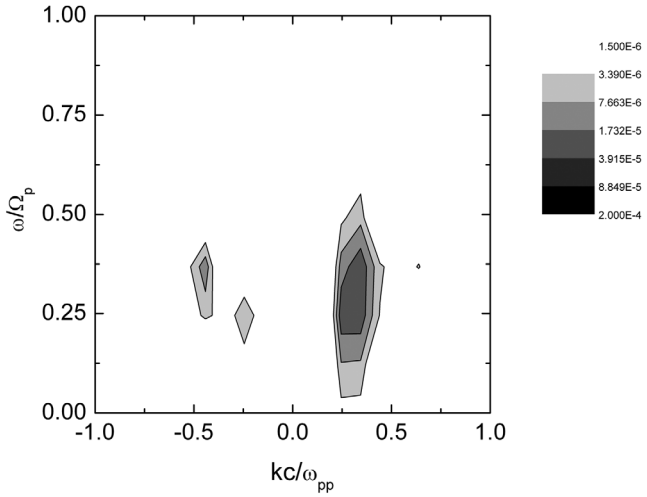

Figure 3. Characteristics of the $\omega - k$ diagram obtained by Fourier transformation of the fluctuating magnetic fields in the y direction from $\Omega_p t = 0$ to $\Omega_p t = 102.4$ for run 1. The positive and negative k represent the forward and backward propagating waves.

The simulation results are presented in section 3. The discussion and conclusions are given in section 4, and their implications on observations are also presented in this section.

2. Simulation Model

[6] In the hybrid simulations the ions are treated kinetically while the electrons are considered as massless fluid [*Winske*, 1985; *Lu and Wang*, 2005b]. The particles are advanced according to the well-known Boris algorithm while the electromagnetic fields are calculated with an implicit algorithm. The plasma consists of three ion components (H^+, He^{2+} and O^{6+}) and the electron component. However, O^{6+} is not considered self-consistently in the simulation model, and it is treated as test particle because of its low number density. He^{2+} contains 4% of total ion number density, which is a typical value in the solar wind. Initially, the electron fluid bears zero average flow speed, and H^+ satisfies bi-Maxwellian velocity distribution. He^{2+} and O^{6+} are assumed to satisfy ring beam distributions and their initial thermal velocities are same as the parallel thermal velocity of H^+, which is consistent with the observations in the solar wind [*Feldman et al.*, 1996; *Gary et al.*, 2001]. According to the injection model of *Fuselier and Schmidt* [1997], the shock can be modeled as an effective potential. Because of their different charge-to-mass ratios, the shock slows H^+ more than the minor ions such as He^{2+} and O^{6+}, which results in a relative velocity between H^+ and the minor ions just downstream of the collisionless shock. The difference of their velocities is called the injection velocity, which can be defined as

$$\mathbf{V}_{inject} = \mathbf{V}_{MI} - \mathbf{V}_H, \tag{1}$$

where $\mathbf{V}_{MI}$ and $\mathbf{V}_H$ are the bulk velocities of the minor ions and H^+ downstream of the shock. The injection angle α is determined from the dot product of the injection velocity with the downstream magnetic field,

$$\alpha = \cos^{-1}\left(\frac{\mathbf{V}_{inject} \bullet \mathbf{B}}{|\mathbf{V}_{inject}||\mathbf{B}|}\right), \tag{2}$$

where $\mathbf{B}$ is the downstream magnetic field. By considering a special case, we can obtain an estimate of the magnitude of the injection velocity at the shock. Assuming a perpendicular shock at the subsolar point, the injection angle is 90°. The minor ions and H^+ in the solar wind are assumed to have the same bulk velocity V_{sw}, and then if the width of potential at the shock is infinite thin, the injection velocity can be described as [*Motschmann and Glassmeier*, 1993; *Fuselier and Schmidt*, 1997]

$$V_{inject} = V_{MI} - V_H = V_{sw}\left(\sqrt{1 - \frac{(q/m)_{MI}}{(q/m)_H}(1 - r^2)} - r\right). \tag{3}$$

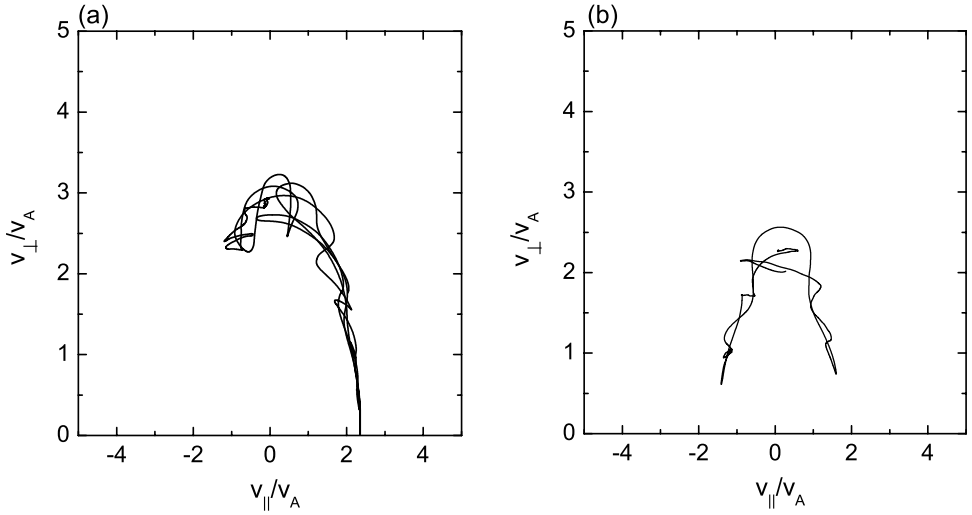

Figure 4. Typical trajectories of (a) He^{2+} and (b) O^{6+} from $\Omega_p t = 0$ to $\Omega_p t = 240$ for run 1.

Here $r = V_H/V_{sw}$ is the compression ratio at the shock. For a supercritical, high Mach number, nearly perpendicular shock, r is about 0.3 and the injection speeds for He^{2+} and O^{6+} are about $0.44|\mathbf{V}_{sw}|$ and $0.51|\mathbf{V}_{sw}|$. In our simulation we choose the injection speeds of He^{2+} and O^{6+} as 2.5 V_A (V_A is the local Alfvén speed) and 2.9 V_A, respectively. The injection angle is $\alpha = 85°$.

[7] Periodic boundary conditions for the particles and fields are used in the simulations. The background magnetic field is assumed to be $\mathbf{B}_0 = B_0\,\hat{\mathbf{x}}$. In the simulations, units of space and time are c/ω_{pp} (where c/ω_{pp} is the proton inertial length, c and ω_{pp} are light speed and proton plasma frequency, respectively) and Ω_p (where $\Omega_p = eB_0/m_p$ is the proton gyro frequency). The number of the grid cells is $n_x = 128$, and the grid size is $\Delta x = 1.0c/\omega_{pp}$ with 1000 particles per cell for each ion component. The time step is taken to be $\Omega_p t = 0.04$. The simulations are performed in the center-of-mass frame, where charge neutrality ($\sum_j e_j n_j = 0$) and the zero current condition ($\sum_j e_j n_j v_{0j} = 0$) are imposed at $t = 0$.

3. Simulation Results

[8] In low beta plasma ($\beta_{\|p} \leq 1$), the He^{2+} ring beam distribution and H^+ distribution with large perpendicular temperature anisotropy can excite helium cyclotron waves and proton cyclotron waves, respectively. Both of them are left-hand polarized waves that can propagate forward and backward, and mirror waves can be neglected in this situation. The simulation parameters used in our 1-D hybrid simulations are listed in Table 1.

[9] Figure 1 shows the time evolution of the amplitude of the fluctuating magnetic field $\delta B^2/B_0^2$ (Figure 1a), the kinetic temperatures for He^{2+} (Figure 1b), and the H^+ temperatures for run 1 (Figure 1c). The temperatures of H^+ and He^{2+} are calculated with the following procedure: we first calculate the temperature in each cell, and the temperature shown in Figure 1 is the average value of all cells. The waves begin to be excited at $\Omega_p t \approx 25$, and saturate at $\Omega_p t \approx 90$. In the linear growth stage, the free energy for the excited ion cyclotron waves is provided mainly by the He^{2+} ring beam distribution, therefore the waves belong to helium cyclotron waves. At the same time, the helium cyclotron waves can heat H^+ in the direction perpendicular to the ambient magnetic field. The H^+ temperature anisotropy $T_{\perp p}/T_{\|p}$ can increase from 1.7 to about 1.8, and then it decrease gradually until to the quasi-equilibrium stage. At the quasi-equilibrium stage, the average amplitude of the helium cyclotron waves is about $\delta B^2/B_0^2 \approx 0.04$, and the temperature anisotropies for H^+ and He^{2+} are about 1.65 and 1.63, respectively. The parallel temperature $T_{\|p}/T_{\|p0}$ for H^+ is almost unchanged.

[10] Figure 2 describes the evolution of the He^{2+} and O^{6+} velocity distributions $f(v_\|, v_\perp)$ at different time for run 1. Initially, both He^{2+} and O^{6+} satisfy ring beam distributions, which concentrate near ($v_\| = 0.22\ v_A$, $v_\perp = 2.49\ v_A$) and ($v_\| = 0.25\ v_A$, $v_\perp = 2.89\ v_A$), respectively. With the excitation of the helium cyclotron waves, He^{2+} is first pitch angle scattered into a shell-like distribution because of its smaller mass than O^{6+}, and then O^{6+} is also scattered into a shell-like distribution. Both the shell-like distributions for He^{2+} and O^{6+} can be formed at the quasi-equilibrium stage, which seems to exist for a long time. The radius of the shell for O^{6+} is larger than that for He^{2+}. The simulation results are consistent with spacecraft observations [*Fuselier et al.*, 1988].

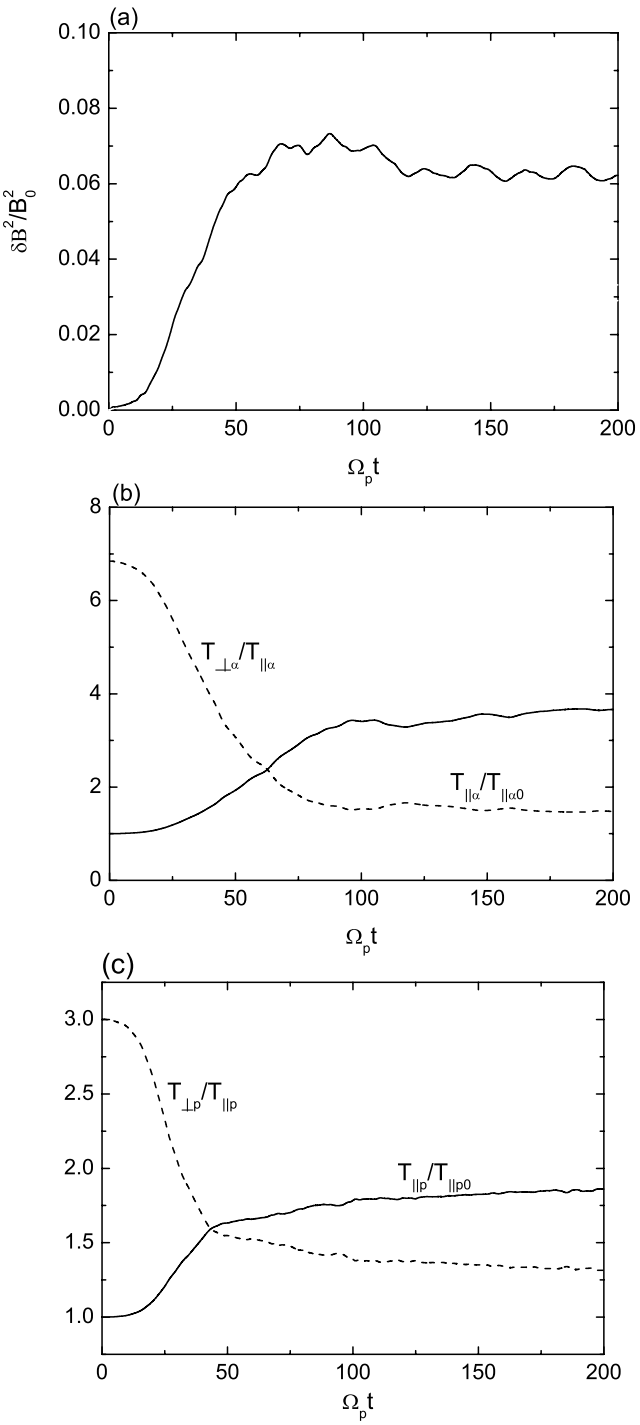

Figure 5. Time evolution of (a) the amplitude of the fluctuating magnetic field $\delta B^2/B_0^2$, (b) the kinetic temperatures for He^{2+}, and (c) the H^+ temperatures for run 2. $T_{\|\alpha 0}$ and $T_{\|p0}$ are the initial parallel temperatures for He^{2+} and H^+.

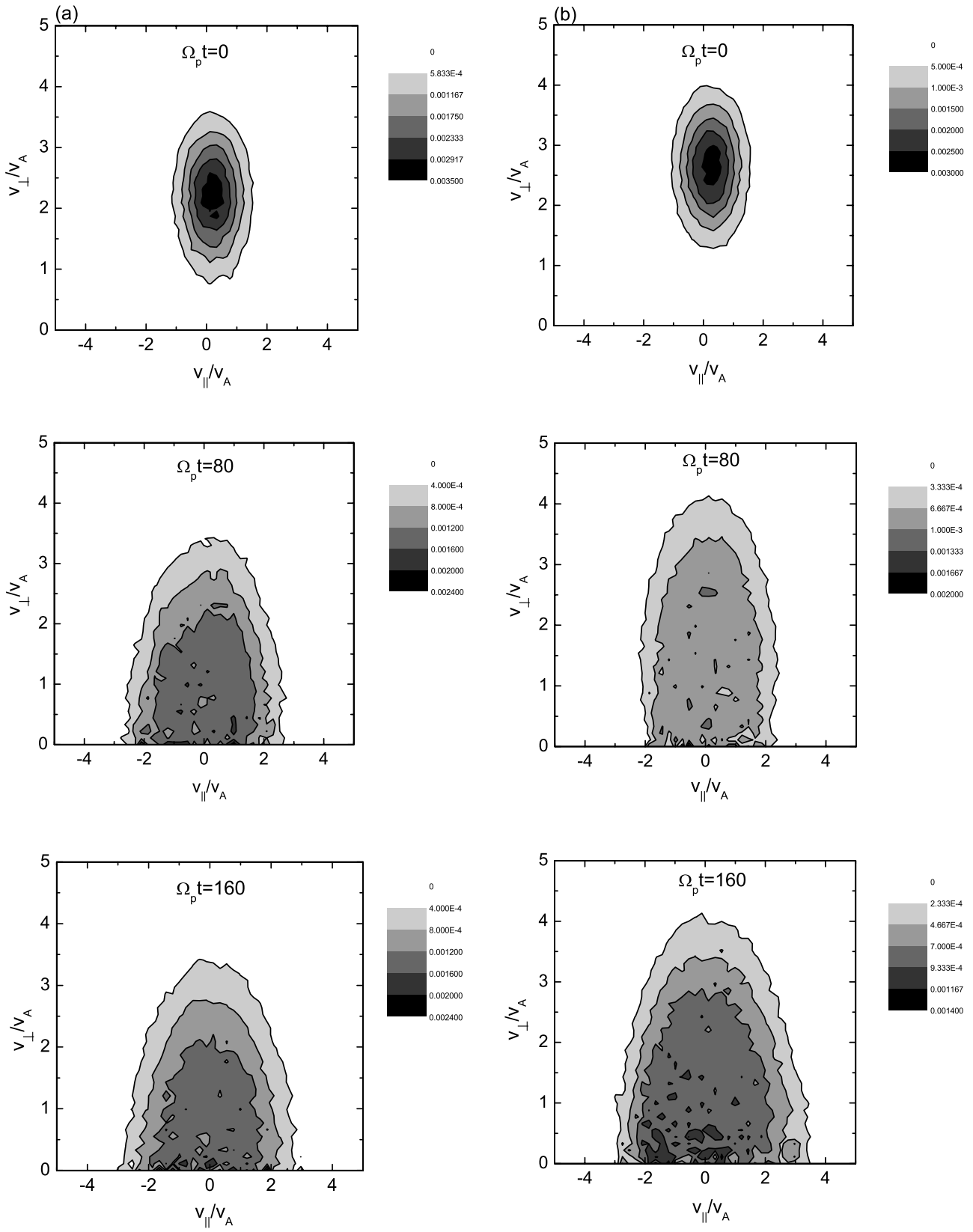

Figure 6. Time evolution of the (a) He^{2+} and (b) O^{6+} velocity distributions $f(v_\parallel, v_\perp)$ at different times for run 2.

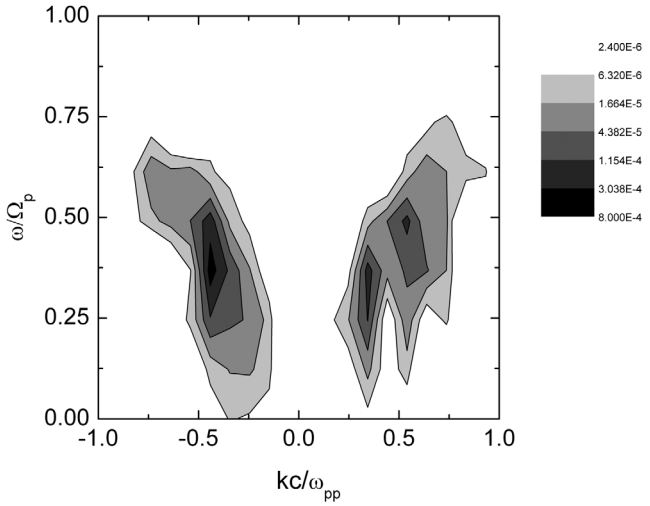

Figure 7. Characteristics of the $\omega - k$ diagram obtained by Fourier transformation of the fluctuating magnetic fields in the y direction from $\Omega_p t = 0$ to $\Omega_p t = 102.4$ for run 2. The positive and negative k represent the forward and backward propagating waves.

[11] The process for the formation of He^{2+} and O^{6+} shell-like distributions through the scattering of the helium cyclotron waves can be understood by investigating the characteristics of waves. Figure 3 shows the characteristics of $\omega - k$ diagram obtained by Fourier transformation of the fluctuating magnetic field in the y direction from $\Omega_p t = 0.0$ to $\Omega_p t = 102.4$ for run 1. From Figure 3, we can find that the waves with both the positive and negative phase speeds are excited, which correspond to the left-hand polarized waves propagating forward and backward, respectively. It is clear that the most power resides near frequency 0.25 Ω_p and wave number is about 0.25 ω_{pp}/c. The frequencies are below the He^{2+} cyclotron frequency, and its dispersion relation can be approximated as $\omega \approx kv_A$ and $\omega \approx -kv_A$ for waves propagating forward and backward, respectively. The ion trajectories scattered by these two branches of waves can be described by the following equations, respectively [*Wu et al.*, 1997]:

$$\left(v_{\parallel} - v_A\right)^2 + v_{\perp}^2 = const \tag{4}$$

$$\left(v_{\parallel} + v_A\right)^2 + v_{\perp}^2 = const. \tag{5}$$

The He^{2+} trajectory passing through ($v_{\parallel} = 0.22\ v_A$, $v_{\perp} = 2.49\ v_A$) and O^{6+} trajectory passing through ($v_{\parallel} = 0.25\ v_A$, $v_{\perp} = 2.89\ v_A$) are also depicted in Figure 2, and they are consistent with the He^{2+} and O^{6+} shell-like distributions obtained in our hybrid simulations. The shell-like distributions for He^{2+} and O^{6+} can be demonstrated in Figure 4, which describes the typical trajectories of He^{2+} and O^{6+} for run 1. It can be found that the motions of $He^{2+}$and O^{6+} are approximately confined on the surfaces of different spheres, thus the assembly of particles will form a shell-like distributions.

[12] First we keep $\beta_{\|p} = 0.5$, and then increase the H^+ temperature anisotropy to investigate its effect on the wave characteristics and He^{2+} and O^{6+} distributions. Figure 5 shows the time evolution of the amplitude of the fluctuating magnetic field $\delta B^2/B_0^2$ (Figure 5a), the kinetic temperatures for He^{2+} (Figure 5b), and the H^+ temperatures for run 2 (Figure 5c). At the quasi-equilibrium stage the average amplitude of ion cyclotron waves is about $\delta B^2/B_0^2 = 0.06$ which is also the combined effect of the proton cyclotron waves and helium cyclotron waves. The amplitude of the proton cyclotron waves is already sufficiently large. The parallel temperature $T_{\|p}/T_{\|p0}$ for H^+ is heated to about 1.85 at the quasi-equilibrium stage. The evolution of the He^{2+} and O^{6+} velocity distributions $f(v_{\|}, v_{\perp})$ for run 2 is presented in Figure 6. No shell-like distributions are formed for either He^{2+} or O^{6+}, and the ring beam distributions of He^{2+} and O^{6+} are pitch angle scattered into nearly bi-Maxwellian distributions at the quasi-equilibrium stage.

[13] Figure 7 shows the characteristics of $\omega - k$ diagram obtained by Fourier transformation of the fluctuating magnetic fields in the y direction from $\Omega_p t = 0.0$ to $\Omega_p t = 102.4$

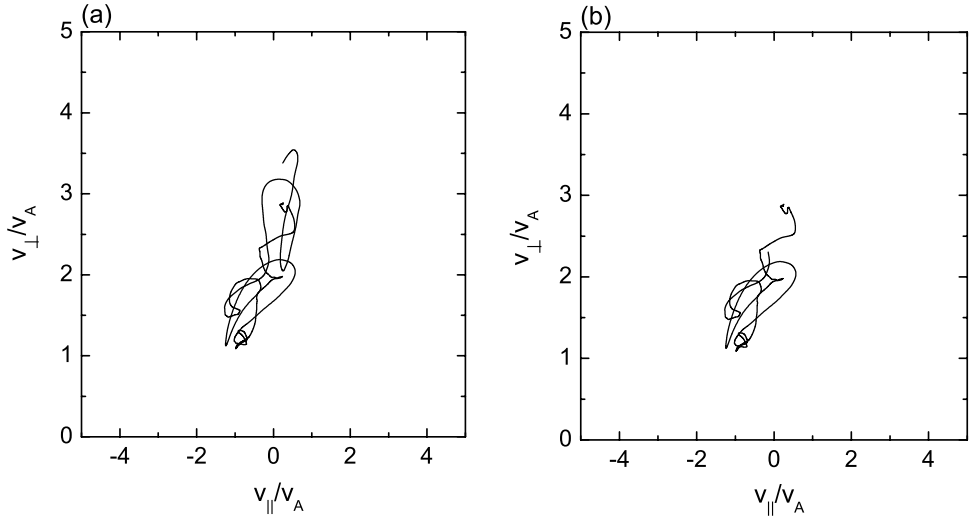

Figure 8. Typical trajectories of (a) He^{2+} and (b) O^{6+} from $\Omega_p t = 0$ to $\Omega_p t = 240$ for run 2.

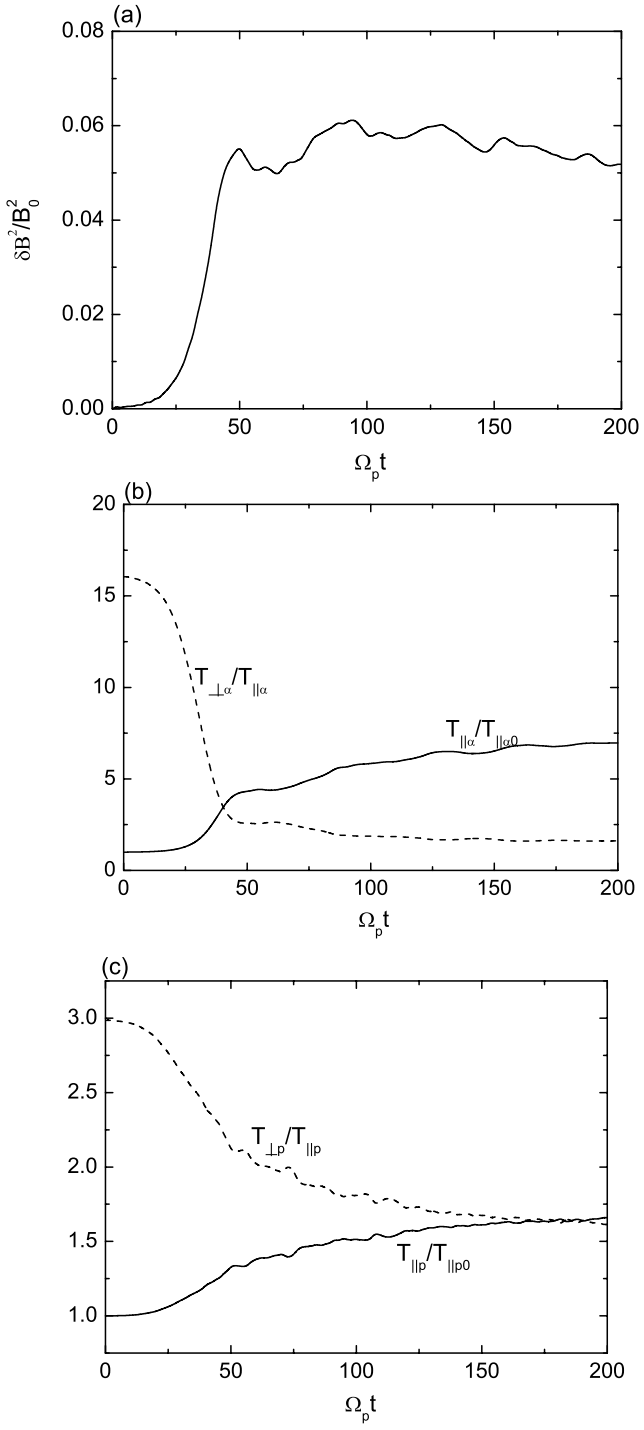

Figure 9. Time evolution of (a) the amplitude of the fluctuating magnetic field $\delta B^2/B_0^2$, (b) the kinetic temperatures for He^{2+}, and (c) the H^+ temperatures for run 3. $T_{\|\alpha 0}$ and $T_{\|p0}$ are the initial parallel temperatures for He^{2+} and H^+, respectively.

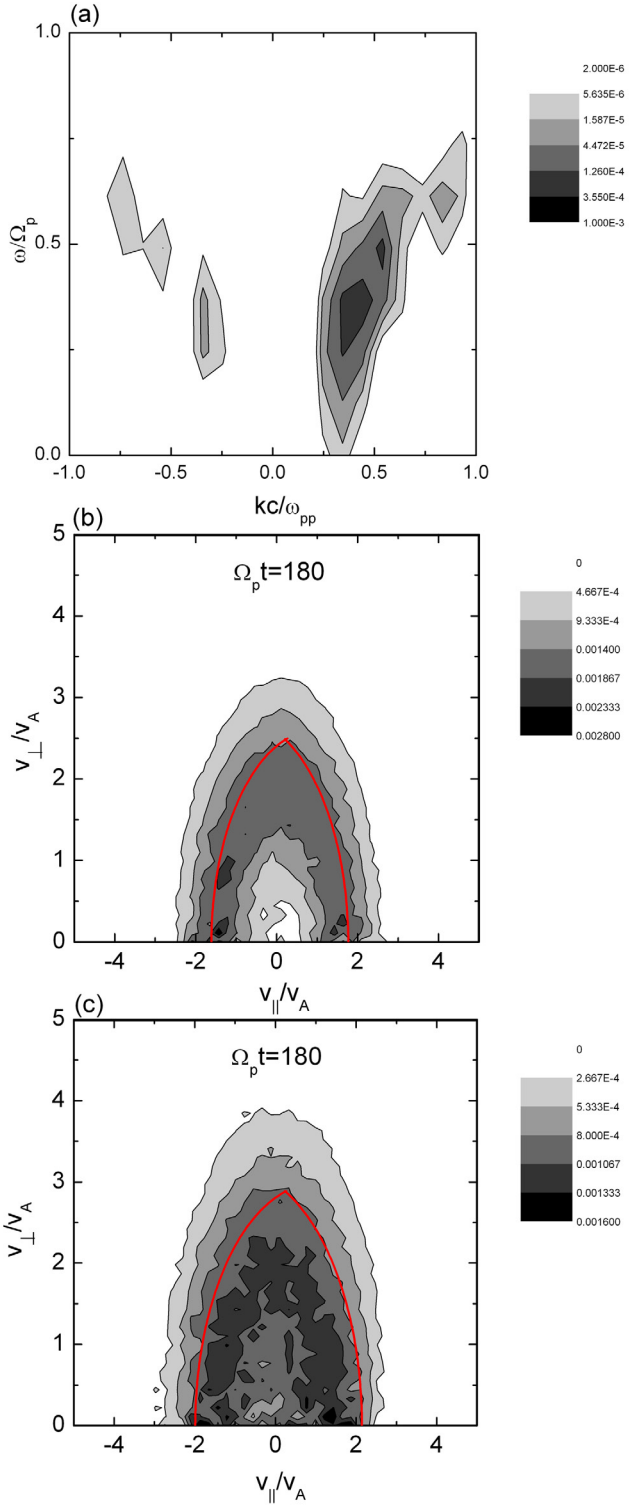

Figure 10. (a) The $\omega - k$ diagram and the (b) He^{2+} and (c) O^{6+} velocity distributions $f(v_\|, v_\perp)$ at $\Omega_p t = 180$ for run 3. The $\omega - k$ diagram is obtained by Fourier transformation of the fluctuating magnetic fields in the y direction from $\Omega_p t = 0.0$ to $\Omega_p t = 102.4$. The red lines denote the He^{2+} and O^{6+} trajectories. The trajectories satisfy equations (4) and (5) at the same time they pass through ($v_\| = 0.22\ v_A$, $v_\perp = 2.49$) and ($v_\| = 0.24\ v_A$, $v_\perp = 2.89\ v_A$) for He^{2+} and O^{6+}, respectively.

for run 2. The waves have broad spectrum and their frequencies exceed the He^{2+} cyclotron frequency and reach about 0.75 Ω_p. The waves are dispersive, which leads to the irregular motions for He^{2+} and O^{6+}. The typical trajectories of He^{2+} and O^{6+} are described in Figure 8, such motions of

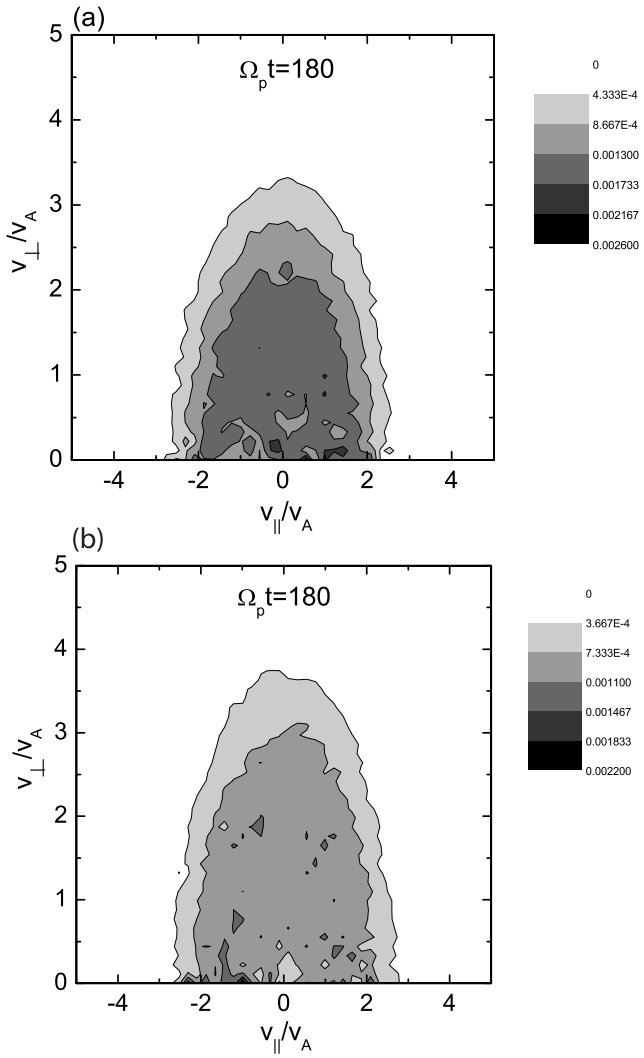

Figure 11. Time evolution of the (a) He^{2+} and (b) O^{6+} velocity distributions $f(v_\parallel, v_\perp)$ at $\Omega_p t = 180$ for run 4.

He^{2+} and O^{6+} result in their bi-Maxwellian at the quasi-equilibrium stage.

[14] We also perform another case with the same parameters as run 2, but treat He^{2+} as test particles. In this way only the proton cyclotron waves are retained, and the effect of the helium cyclotron waves is eliminated. In this way, we can determine which factor, the proton cyclotron waves or the combined effect of the proton cyclotron waves and helium cyclotron waves, scatters He^{2+} and O^{6+} from ring beam distributions into bi-Maxwellian distributions. The results show that the proton cyclotron waves can scatter He^{2+} and O^{6+} from ring beam distributions into bi-Maxwellian functions (not shown). So we conclude that the helium cyclotron waves can scatter He^{2+} and O^{6+} from ring beam distributions into shell-like distributions while the proton cyclotron waves tend to scatter them into bi-Maxwellian distributions.

[15] Next, we investigate the effect of the plasma beta $\beta_{\parallel p}$ on the excited waves. Figure 9 describes the time evolution of the amplitude of the fluctuating magnetic field $\delta B^2/B_0^2$ (Figure 9a), the kinetic temperatures for He^{2+} (Figure 9b), and the H^+ temperatures for run 3 (Figure 9c). In this case, both the helium cyclotron waves and proton cyclotron waves are also excited. At the quasi-equilibrium stage, the average amplitude of ion cyclotron waves is about $\delta B^2/B_0^2 = 0.05$. Figure 10 describes the $\omega - k$ diagram (Figure 10a), the He^{2+} (Figure 10b), and O^{6+} velocity distributions $f(v_\parallel, v_\perp)$ at $\Omega_p t = 180$ for run 3 (Figure 10c). In Figure 10, the $\omega - k$ diagram is obtained by Fourier transformation of the fluctuating magnetic field in the y direction from $\Omega_p t = 0.0$ to $\Omega_p t = 102.4$. Similar to run 2, we can find that both the proton cyclotron waves and the helium cyclotron waves are excited. However, the He^{2+} and O^{6+} shell-like distributions are still formed at the quasi-equilibrium stage. If we increase the H^+ temperature anisotropy, the He^{2+} and O^{6+} shell-like distributions disappear at about $T_{\perp p}/T_{\parallel p} = 4.5$. Figure 11 describes the He^{2+} and O^{6+} velocity distributions $f(v_\parallel, v_\perp)$ at $\Omega_p t = 180$ for run 4, the shell-like distributions disappear, and the He^{2+} and O^{6+} distributions satisfy nearly bi-Maxwellian function.

[16] If the plasma beta $\beta_{\parallel p}$ is increased, we must decrease the H^+ temperature anisotropy to obtain the He^{2+} and O^{6+} shell-like distributions. For $\beta_{\parallel p} = 0.8$, the He^{2+} and O^{6+} shell-like distributions are only formed when $T_{\perp p}/T_{\parallel p}$is near 1.0. Figure 12 shows the He^{2+} and O^{6+} velocity distributions $f(v_\parallel, v_\perp)$ at $\Omega_p\ t = 180$ for run 5, there still exist shell-like distributions for He^{2+} and O^{6+}. However, if we further increases $\beta_{\parallel p}$ to be larger than 0.9, the shell-like distributions cannot be formed no matter what value of $T_{\perp p}/T_{\parallel p}$is chosen.

4. Discussion and Conclusions

[17] Both observations and computer simulations show that H^+ downstream of a quasi-perpendicular shock has larger perpendicular temperature. In addition to this, the incident solar wind H^+ and other minor ions (such as He^{2+} and O^{6+}) slow differentially across the boundary of a shock because of their different charge-to-mass ratios. It leads to ring beam distributions for the minor ions downstream of quasi-perpendicular shocks. In this paper, using one-dimensional hybrid simulations, we investigate the competition between the proton cyclotron waves and helium cyclotron waves downstream of quasi-perpendicular shocks, which are excited by the H^+ temperature anisotropy and He^{2+} ring beam distributions, respectively. Helium cyclotron waves have narrow spectrum and their frequency is below the He^{2+} cyclotron frequency, their characteristics are similar to that excited by He^{2+} temperature anisotropy [*Denton et al.*, 1993, 1994; *Gary et al.*, 1994; *Gnavi et al.*, 2000]. The motions of He^{2+} and O^{6+} are approximately confined on the surface of a sphere, which result in their shell-like distributions downstream of quasi-perpendicular shocks. With the increase of H^+ temperature anisotropy while $\beta_{\parallel p}$ kept as a constant, the amplitude of the excited proton cyclotron waves increases. The power spectrum of the proton cyclotron waves is broad and their frequency can exceed the He^{2+} cyclotron frequency. When the proton cyclotron waves are sufficiently strong and comparable to the helium cyclotron waves. The motions of He^{2+} and O^{6+} are irregular and it results in their bi-Maxwellian distributions at the quasi-equilibrium stage. Our results also show that the He^{2+} and O^{6+} shell-like distributions are easily formed when the plasma beta $\beta_{\parallel p}$ is small.

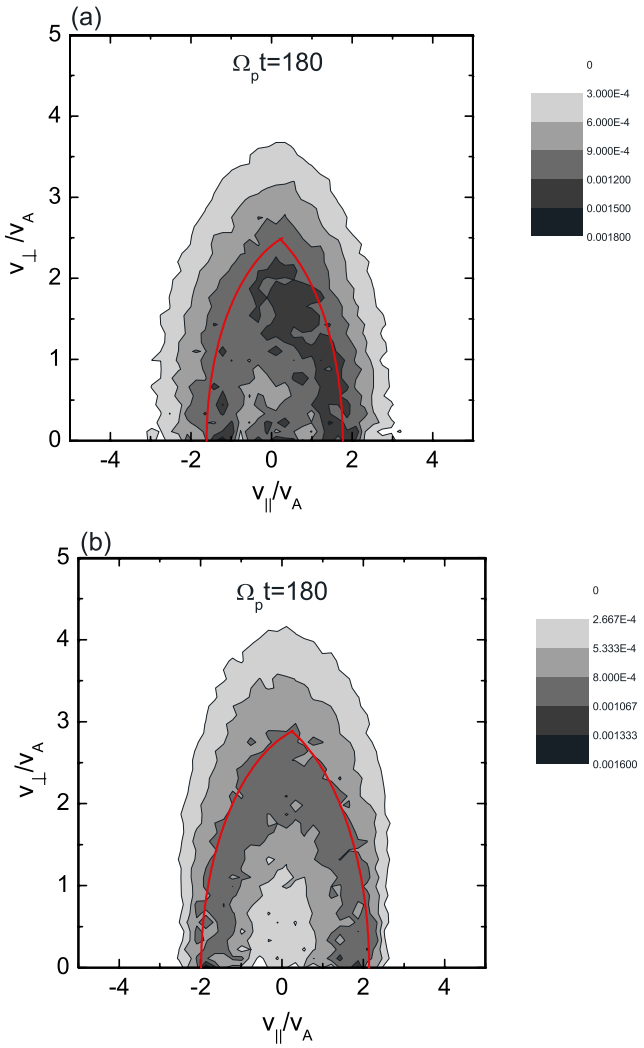

Figure 12. (a) He^{2+} and (b) O^{6+} velocity distributions $f(v_\parallel, v_\perp)$ at $\Omega_p\, t = 180$ for run 5. The red lines denote the He^{2+} and O^{6+} trajectories. The trajectories satisfy equations (4) and (5) at the same time they pass through ($v_\parallel = 0.22\ v_A$, $v_\perp = 2.49\ v_A$) and ($v_\parallel = 0.24\ v_A$, $v_\perp = 2.89\ v_A$) for He^{2+} and O^{6+}, respectively.

[18] The helium cyclotron waves have characteristics similar to the proton cyclotron waves, but they have narrow spectrum. No direct evidences for the existence of the helium cyclotron waves downstream of quasi-perpendicular shocks have been reported. *Fuselier and Schmidt* [1997] observed He^{2+} and O^{6+} ring beam distributions immediately downstream of shocks. The AMPTE/CCE spacecraft has presented simultaneous observations of shell-like distributions for He^{2+} and O^{6+} in the magnetosheath, and O^{6+} has larger radius than He^{2+} [*Fuselier et al.*, 1988]. Our simulation results show that the helium cyclotron waves tend to scatter He^{2+} and O^{6+} from ring beam distributions into shell-like distributions, while the proton cyclotron waves will scatter them into bi-Maxwellian distributions. Only when the electromagnetic waves are predominated by the helium cyclotron waves, the He^{2+} and O^{6+} shell-like distributions are formed downstream of shocks. Therefore we can infer that there exist helium cyclotron waves downstream of quasi-perpendicular shocks, which are excited by He^{2+} ring beam distributions.

[19] In our simulations, we assume that the shock is an infinite thin electrostatic potential and it is not self-consistently included in our model. *McKean et al.* [1995b, 1996] have studied the evolution of waves and particles downstream of a quasi-perpendicular shock with 2-D hybrid simulation. In their model, the shock is considered consistently, and H^+ and He^{2+} ion components are considered. Nearly all He^{2+} are directly transmitted and forms a nongyrotropic ring distribution immediately downstream of the shock in the downstream frame, which is consistent with our assumption. However, in their simulations the following He^{2+} dynamics is controlled by the proton cyclotron waves and are heated in the direction perpendicular to the ambient magnetic field. These results are similar to our cases where the waves are predominated by the proton cyclotron waves, which have already been studied by *Omura et al.* [1985]. The heating of protons and minor ions across a quasi-perpendicular shock has also been investigated with one-dimensional hybrid simulations, and is applied to explain the coronal heating [*Lee and Wu*, 2000; *Lee*, 2001]. Because there are observed He^{2+} and O^{6+} shell-like distributions downstream of shocks and only the helium cyclotron waves can scatter them from ring beam distributions to shell-like distributions, we do believe that the helium cyclotron waves play an important role in some situations. To investigate the role of the helium cyclotron waves in downstream waves of quasi-perpendicular shocks with a simulation model, which includes the shock self-consistently, is our future work.

[20] **Acknowledgments.** This research was supported by the National Science Foundation of China (NSFC) under grants 40574063, 40304012, and 40404012 and Chinese Academy of Sciences grant KZCX3-SW-144.
[21] Lou-Chuang Lee thanks Peter Yoon and the other reviewer for their assistance in evaluating this paper.

References

Anderson, B. J., and S. A. Fuselier (1993), Magnetic pulsations from 0.1 to 4.0 Hz and associated plasma properties in the Earth's subsolar magnetosheath and plasma depletion layer, *J. Geophys. Res.*, *98*, 1461–1479.
Anderson, B. J., S. A. Fuselier, and D. Murr (1991), Electromagnetic ion cyclotron waves observed in the plasma depletion layer, *Geophys. Res. Lett.*, *18*, 1955–1958.
Anderson, B. J., S. A. Fuselier, S. P. Gary, and R. E. Denton (1994), Magnetic spectral signatures in the Earth's magnetosheath and plasma depletion layer, *J. Geophys. Res.*, *99*, 5877–5891.
Brinca, A. L., N. Sckopke, and G. Paschman (1990), Wave excitation downstream of low-β, quasi-perpendicular bow shock, *J. Geophys. Res.*, *95*, 6331–6335.
Denton, R. E., M. K. Hudson, S. A. Fuselier, and B. J. Anderson (1993), Electromagnetic ion cyclotron waves in the plasma depletion layer, *J. Geophys. Res.*, *98*, 13,477–13,490.
Denton, R. E., S. P. Gary, B. J. Anderson, S. A. Fuselier, and M. K. Hudson (1994), Low-frequency magnetic fluctuation spectra in the magnetosheath and plasma depletion layer, *J. Geophys. Res.*, *99*, 5893–5902.
Feldman, W. C., B. L. Barraclough, J. L. Phillips, and Y. M. Wang (1996), Constraints on high-speed solar wind structures near its coronal base: A Ulysses perspective, *Astron. Astrophys.*, *316*, 355–367.
Fuselier, S. A., and W. K. H. Schmidt (1997), Solar wind He^{2+} ring-beam distributions downstream from the Earth's bow shock, *J. Geophys. Res.*, *102*, 11,273–11,280.
Fuselier, S. A., E. G. Shelley, and D. M. Klumpar (1988), AMPTE/CCE observations of the shell-like He^{2+} and O^{6+} distributions in the magnetosheath, *Geophys. Res. Lett.*, *15*, 1333–1336.
Fuselier, S. A., D. M. Klumpar, E. G. Shelley, B. J. Anderson, and A. J. Coates (1991), He^{2+} and H^+ dynamics in the subsolar magnetosheath and plasma depletion layer, *J. Geophys. Res.*, *96*, 21,095–21,104.

Gary, S. P. (1992), The mirror and ion cyclotron anisotropy instabilities, *J. Geophys. Res.*, *97*, 8519–8529.

Gary, S. P., S. A. Fuselier, and B. J. Anderson (1993), Ion anisotropy instabilities in the magnetosheath, *J. Geophys. Res.*, *98*, 1481–1488.

Gary, S. P., P. D. Convery, R. E. Denton, S. A. Fuselier, and B. J. Anderson (1994), Proton and helium cyclotron anisotropy instability thresholds in the magnetosheath, *J. Geophys. Res.*, *99*, 5915–5921.

Gary, S. P., B. E. Goldstein, and J. T. Steinberg (2001), Helium ion acceleration and heating by Alfvén/cyclotron fluctuations in the solar wind, *J. Geophys. Res.*, *106*, 24,955–24,963.

Gnavi, G., F. T. Gratton, and C. J. Farrugia (2000), Theoretical properties of electromagnetic ion cyclotron waves in the terrestrial, dayside, low-latitude plasma depletion layer under uncompressed magnetosheath conditions, *J. Geophys. Res.*, *105*, 20,973–20,987.

Lee, L. C. (2001), A new mechanism of coronal heating, *Space Sci. Rev.*, *95*, 95–106.

Lee, L. C., and B. H. Wu (2000), Heating and acceleration of protons and minor ions by fast shocks in the solar corona, *Astrophys. J.*, *535*, 1014–1026.

Lee, L. C., C. P. Price, C. S. Wu, and M. E. Mandt (1988), A study of mirror waves generated downstream of a quasi-perpendicular shock, *J. Geophys. Res.*, *93*, 247–250.

Leroy, M. M., D. Winske, C. C. Goodrich, C. S. Wu, and K. Papadopoulos (1982), The structure of perpendicular bow shock, *J. Geophys. Res.*, *87*, 5081–5094.

Lin, Y., and X. Y. Wang (2002), Simulation of ion velocity distributions in the magnetosheath, *Geophys. Res. Lett.*, *29*(14), 1687, doi:10.1029/2002GL015100.

Liu, Y. C.-M., M. A. Lee, and H. Kucharek (2005), A quasilinear theory of ion "thermalization" and wave excitation downstream of Earth's bow shock, *J. Geophys. Res.*, *110*, A09101, doi:10.1029/2005JA011096.

Lu, Q. M., and S. Wang (2005a), Formation of He^{2+} shell-like distributions downstream of the Earth's bow shock, *Geophys. Res. Lett.*, *32*, L03111, doi:10.1029/2004GL021508.

Lu, Q. M., and S. Wang (2005b), Proton and He^{2+} temperature anisotropies in the solar wind driven by ion cyclotron waves, *Chin. J. Astron. Astrophys.*, *5*, 184–192.

Lu, Q. M., F. Guo, and S. Wang (2006), Magnetic spectral signatures in the terrestrial plasma depletion layer: Hybrid simulations, *J. Geophys. Res.*, *111*, A04207, doi:10.1029/2005JA011405.

McKean, M. E., D. Winske, and S. P. Gary (1992), Mirror and ion cyclotron anisotropy instabilities in the magnetosheath, *J. Geophys. Res.*, *97*, 19,421–19,432.

McKean, M. E., N. Omidi, and D. Krauss-Varban (1995a), Wave and ion evolution downstream of quasi-perpendicular bow shocks, *J. Geophys. Res.*, *100*, 3427–3437.

McKean, M. E., N. Omidi, D. Krauss-Varban, and H. Karimabadi (1995b), Wave and particle evolution downstream of quasi-perpendicular shocks, *Adv. Space Res.*, *15*, 319–322.

McKean, M. E., N. Omidi, and D. Krauss-Varban (1996), Magnetosheath dynamics downstream of low Mach number shocks, *J. Geophys. Res.*, *101*, 20,013–20,022.

Motschmann, U., and K. H. Glassmeier (1993), Simulation of heavy ion ring and shell distributions downstream of the bow shock, *Geophys. Res. Lett.*, *20*, 987–990.

Omura, Y., M. Ashour-Abdalla, R. Gendrin, and K. Quest (1985), Heating of thermal helium in the equatorial magnetopause: A simulation study, *J. Geophys. Res.*, *90*, 8281–8292.

Peterson, W. K., E. G. Shelley, R. D. Sharp, R. G. Johnson, J. Geiss, and H. Rosenbauer (1979), H^+ and He^{2+} in the dawnside magnetosheath, *Geophys. Res. Lett.*, *6*, 667–670.

Price, C. P., D. W. Swift, and L. C. Lee (1986), Numerical simulation of nonoscillatory mirror waves at the Earth's magnetosheath, *J. Geophys. Res.*, *91*, 101–112.

Sckopke, N., G. Paschmann, A. L. Brinca, C. W. Carlson, and H. Luhr (1990), Ion thermalization in quasi-perpendicular shocks involving reflected ions, *J. Geophys. Res.*, *95*, 6337–6348.

Tanaka, M. (1985), Simulations of heavy-ion heating by electromagnetic ion-cyclotron waves driven by proton temperature anisotropies, *J. Geophys. Res.*, *90*, 6459–6468.

Winske, D. (1985), Hybrid simulation codes with applications to shocks and upstream waves, *Space Sci. Rev.*, *42*, 53–66.

Winske, D., and K. B. Quest (1988), Magnetic field and density fluctuations at perpendicular supercritical collisionless shocks, *J. Geophys. Res.*, *93*, 9681–9693.

Wu, C. S., P. H. Yoon, and J. K. Chao (1997), Motion of ions influenced by enhanced Alfven waves, *Phys. Plasmas*, *4*, 856–862.

Yoon, P. H. (1992), Quasi-linear evolution of Alfven-ion-cyclotron and mirror instabilities driven by ion temperature anisotropy, *Phys. Fluids B*, *4*, 3627–3637.

Q. M. Lu and S. Wang, CAS Key Laboratory of Basic Plasma Physics, School of Earth and Space Sciences, University of Science and Technology of China, Hefei, Anhui 230026, China. (qmlu@ustc.edu.cn)